Microstructural Evaluation and Property Change of 5 Wt Pct Al-Zn Coating on Press Hardening Steel During Austenitization

JUN-KAI CHANG, CHAO-SUNG LIN, WOEI-REN WANG, and WEI-JEN CHENG

Microstructural evolution of a 5 wt pct Al-Zn coating on press hardening steel was studied in comparison to hot-dip galvanized (GI) and galvannealed (GA) coatings. The results show that the presence of 5 wt pct Al effectively suppresses oxidation during austenitization; meanwhile, the presence of Fe resulting from galvannealing accelerates oxidation. Alloying with Al or Fe in the coating prior to austenitization reduces the susceptibility to liquid metal embrittlement (LME). The presence of Al in the as-coated Zn coating enhances the corrosion resistance in HCl solution and reduces the cathodic kinetics in NaCl solution. However, for sacrificial protection, the austenitized GI steel outperforms the other austenitized-coated steels. Nevertheless, the 5 wt pct Al-Zn coating exhibits better overall performance including high-temperature oxidation resistance, less LME susceptibility, and cathodic protection.

https://doi.org/10.1007/s11661-018-4694-0

I. INTRODUCTION

ADVANCED high-strength steels (AHSS), including dual-phase steel, twinning-induced plasticity steel, complex phase steel, and martensitic ultrahigh-strength steel (MART steel), have found many applications in the automobile industry for developing lightweight vehicles to meet demands of reduction in fuel consumption and carbon dioxide emissions.[1–4] Specifically, the AHSS sheets are applied in car cage parts, such as body-pillars, bumpers, door beams, as well as roof rails, and passenger survival in crash events is better ensured.[5] Hot stamping process is used to fabricate MART steel parts to avoid springback associated with the conventional cold forming technology.[6,7] Press hardening steel, like MnB steel, has been increasingly used in the automobile industry because its strength can be raised from 400 MPa to 1500 ~ 1600 MPa after rapid cooling in the forming die.[8–13] Prior to press forming, the press hardening steel is generally heat treated at 880 ~ 950 °C for 3 ~ 10 minutes,[12,13] when severe oxidation and decarburization occur.[12–14] Therefore, surface modification to form a protective coating is essential for press hardening steel.

Hot-dip aluminizing and galvanizing are commonly employed to fabricate corrosion protective coatings on sheet steels.[14–16] Al-10 wt pct Si coating is the widely used coating on press hardening steel and has been patented as Usibor by ArcelorMittal Corporation.[17] This coating can withstand oxidation and decarburization during the austenitization treatment *via* the formation of an Al_2O_3 layer.[17–19] Although the coating formed after hot stamping offers barrier protection, it only imparts limited sacrificial protection afforded by the resulting Fe-Al intermetallic phases.[20] The protection of such a Fe-Al diffusion layer is not sufficient under harsh corrosion environments.[18–22]

Zn-based coating on steel is known to provide both barrier protection and sacrificial protection.[14,23,24] However, the process temperature of austenitization is markedly higher than the melting point of Zn (419.5 °C). The molten Zn layer suffers extensive oxidation and evaporation.[25–27] The ZnO scale is evident and deteriorates the resistance spot weldability of the steel parts.[14,28,29] Molten Zn(Fe) also quickly reacts with the steel substrate, leading to the formation of Zn-saturated α-Fe [α-Fe(Zn)] and, if present, few amounts of the Fe_3Zn_{10} (Γ) phase. The Zn content of the coating layer has been substantially reduced and the sacrificial protection capability also decreases although the coating layer still offers barrier protection.[17,25,26] Moreover, molten Zn (usually with dissolved Fe) contacting the steel substrate can cause liquid metal

JUN-KAI CHANG and CHAO-SUNG LIN are with the Department of Materials Science and Engineering, National Taiwan University, 1, Roosevelt Road, Section 4, Taipei 106, Taiwan. Contact e-mail: csclin@ntu.edu.tw WOEI-REN WANG is with the Division of Metallic Materials Research, Material and Chemical Research Laboratories, Department of Additive Manufacturing Materials & Applications, Industrial Technology Research Institute, Tainan 709, Taiwan. WEI-JEN CHENG is with the Department of Iron & Steel Research and Development, China Steel Corporation, 1, Chung Kang Road, Kaohsiung 820, Taiwan.

Manuscript submitted September 27, 2017.
Article published online May 31, 2018

embrittlement (LME) as a press forming load is applied.[14,30–33]

The 55 wt pct Al-Zn-coated steel[34,35] and 5 wt pct Al-Zn[36–38]-coated steel are known as Galvalume® and Galfan®, respectively. The eutectic structure composed of Al-rich and Zn-rich phases enhances the corrosion resistance compared to the pure Zn coating. Galvalume® and Galfan® are thus widely applied for architectural and constructional steel structures.[24,34–38] Recently, the oxidation and phase transformation of a 55 wt pct Al-Zn coating on low-carbon steel and press hardening steel have been studied to evaluate its practicability as a protective coating for press hardening steel.[39–41] It has been shown that the coating has transformed to Fe-Al phases and the Zn content has been markedly reduced with Zn remnant residing along the Fe-Al grain boundaries or present as solid solute in Fe-Al phases.[40,41] The LME is thus avoided; however, the sacrificial protection of the resultant alloy layer has not been fully explored. The eutectic reaction of Zn-Al binary alloy system occurs approximately at 382 °C and 5.1 wt pct Al. As a result, the Galfan® coating is generally processed at temperatures lower than those for Galvalume® coating. In this study, the microstructural evolution of a 5 wt pct Al-Zn coating on press hardening steel with and without galvannealing at 500 °C for 25 seconds during austenitization was investigated. The feasibility of the 5 wt pct Al-Zn coating as a protective coating for press hardening steel was evaluated and discussed in detail.

II. EXPERIMENTAL PROCEDURE

A. *Materials*

The steel studied was commercial cold-rolled press hardening steel with thickness of 1.2 mm produced by the China Steel Corporation (CSC), Kaohsiung, Taiwan. The chemical composition of the press hardening steel can be found elsewhere[9] and is typical of 22MnB5 steel. The hot-dip galvanized press hardening steel was prepared using a hot-dip simulator of the CSC. The steel strip was annealed at 1073 K (800 °C) for 60 seconds under N_2-10 pct H_2 atmosphere with a dew point of 213 K ~ 203 K (− 60 °C to − 70 °C). The steel strip was then cooled down to 743 K (470 °C), isothermally held for 30 s, and subsequently dipped into a molten Zn bath containing 0.14 wt pct Al and 5 wt pct Al, respectively, at 723 K (450 °C) for 3 seconds. After being withdrawn from the Zn bath, one coupon was cooled to room temperature at a cooling rate of approximately − 10 K s^{-1} using nitrogen gas, and denoted as the GI specimen because commercial hot-dip Zn coating is commonly recognized as GI coating. The other one was consecutively heated up to 773 K (500 °C), isothermally held for 25 seconds, then cooled down to room temperature at − 10 K s^{-1} using nitrogen gas. This was denoted as the GA specimen, where the GA stands for the galvannealing process employed in the industry to transform the pure Zn coating to a Fe-Zn alloy coating. The specimen was denoted according to the type of Zn bath, hot dipping, and galvannealing process. For example, GI represented the coating made in the Zn bath containing 0.14 wt pct Al and rapidly cooled to room temperature and 5Al-GA represented the coating made in the Zn bath containing 5 wt pct Al and galvannealed at 773 K (500 °C) isothermally for 25 seconds. Figure 1 shows the full temperature history of the hot dipping and galvannealing process, as well as the various specimens produced.

To simulate the austenitization treatment during the hot stamping process, the coated steel was heat treated at 1183 K (910 °C) in an electric furnace for 5 minutes. After the heat treatment, all steels were withdrawn and immediately placed on a cast iron block, which had been sprayed with liquid nitrogen, to simulate the rapid cooing in hot stamping.

A Gleeble 3500 thermal-mechanical process simulator was employed for the elevated temperature tensile test under ambient atmosphere. Figure 2 shows the geometry of the specimen for the tensile test at elevated temperatures reprinted from the ASTM standard.[42,43] A high-temperature axial extensometer was equipped in the center of the specimen. The gauge length of the specimen was 25 mm. The specimen was heated at a rate of 20 K s^{-1} to 1183 K (910 °C) and soaked until a total heating time of 5 minutes, when the specimen was pulled at a strain rate of 0.5 s^{-1} until the specimen had fractured.

B. *Microstructure Analyses*

The crystallinity and phase of the coating and corrosion products (oxides) were identified using X-ray Diffraction (XRD, Rigaku TTRAX 3) with monochromatic Cu-Kα (λ = 1.54439 Å) radiation at 30 kV and 50 mA. The scanning speed was 4 deg min^{-1}. The crystallographica search-match 2.1 software was employed to analyze the characteristic peaks and each phase was identified using the PDF-2 database.[44]

To prepare the cross-sectional specimen for scanning electron microscope (SEM) characterization, two small pieces of the coated steel were glued face-to-face with an G1 epoxy and cured on a hot plate at 473 K (200 °C) for 30 minutes. Cross-sectional slices were then cut by a low-speed diamond saw and mechanically ground using SiC paper up to 4000 grit, followed by polishing using diamond paste down to 0.5 μm. Field-emission gun SEM (FEG-SEM, Nova Nano SEM 450) was used to characterize the microstructure of the coated steels first. The cross section was characterized using backscattered electron (BSE) mode at 25 kV. Chemical composition of the coating and corrosion products was analyzed using the energy dispersive spectrometry (EDS) equipping in the FEG-SEM. For the detailed element distribution on the diffusion layer formed after austenitization, an electron probe X-ray microanalyzer (EPMA, JEOL JXA-8200) was also used to analyze the chemical composition distribution by mapping at 15 kV and 5×10^{-8} A.

The cross-sectional transmission electron microscope (TEM) specimen was extracted from the panel using the focused ion beam technique (FIB, FEI Helios 600i). The

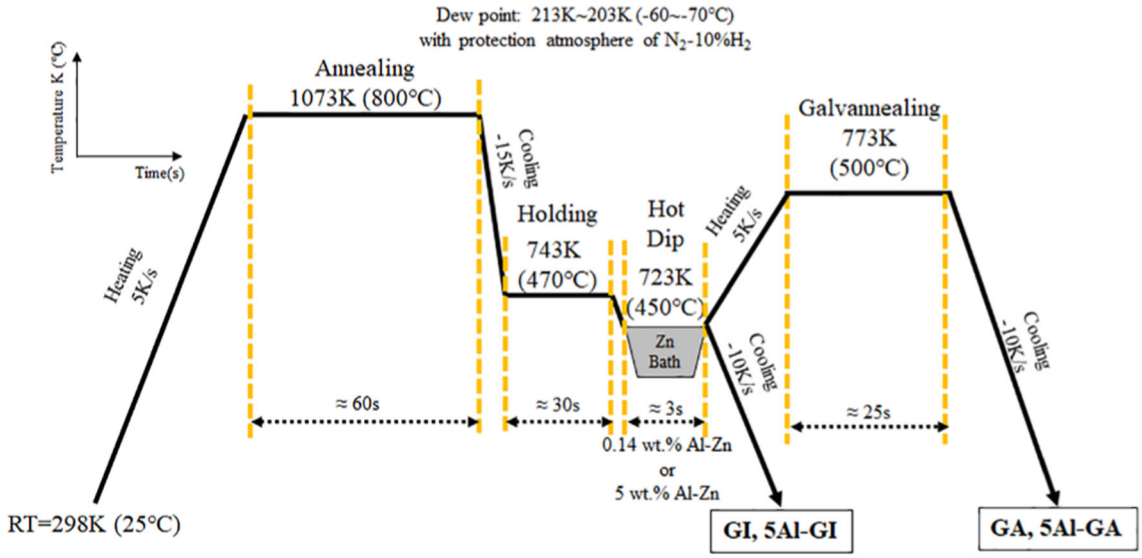

Fig. 1—The temperature history of hot-dip galvanizing/galvannealing process and the various specimens studied.

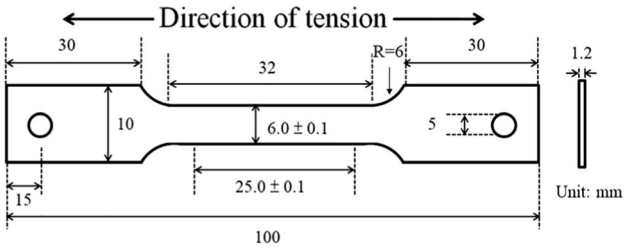

Fig. 2—The geometry of the specimen for tensile test at elevated temperatures (in accordance with the ASTM E8/E8M standard[43]).

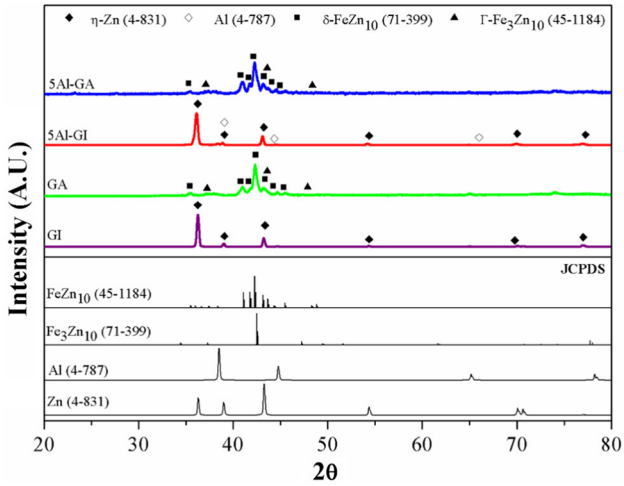

Fig. 3—XRD patterns of the as-coated press hardening steels.

characterization of the oxide layer was carried out using a field-emission TEM (FE-TEM, FEI Tecnai G^2 F20) operating at 200 kV and the attached EDS.

An X-ray photoelectron spectroscope (XPS, AVG Thermo K-Alpha) with an Al Kα monochromatic X-ray source was used for further studying the composition and valence state of the surface oxide scale. The depth profile was also obtained using argon sputtering at an area of approximately 2×1 mm^2. A total depth of approximately 200 nm was recorded in reference to an etching rate of 0.31 nm s^{-1} for SiO_2.

C. *Electrochemical Measurements*

The corrosion behavior of the coated press hardening steel before and after austenitization was first evaluated using an electrochemical stripping method. The test was performed *via* a PARSTAT 4000 potentiostat/galvanostat using a conventional three-electrode cell in 4 wt pct HCl solution at 298 K (25 °C).[45] The corrosion resistance was further studied using potentiodynamic polarization experiments in 0.1 M NaCl solution at 298 K (25 °C). The coated steel with an exposure area of 1.77 cm^2 was employed as the working electrode, and a platinum plate of 16 cm^2 and a saturated calomel electrode (SCE) were used as the counter and reference electrodes, respectively. The polarization curve was measured by sweeping the potential from − 250 to 500 mV relative to the open circuit potential (OCP) at a scan rate of 0.167 mV s^{-1} after the steady OCP of the tested specimen was reached, namely the potential vibration was less than 5 mV over a time period of 300 seconds.

III. RESULTS

A. *Microstructure of the Coating Before Austenitization*

Figure 3 shows the XRD patterns of the various as-coated steels. The GI coating was mainly composed of the Zn terminal solid solution (η-Zn phase); whereas the GA coating consisted of the $FeZn_{10}$ (δ-$FeZn_{10}$ phase) as the major phase and the Fe_3Zn_{10} (Γ-Fe_3Zn_{10} phase) as a minor phase, which results from the interdiffusion of Fe and Zn during galvannealing. All

the peaks of the 5Al-GI coating can be identified to result from the η phase. The peaks associated with the Al were not readily discerned and accurately identified. This is because there is a eutectic point at approximately 5.1 wt pct Al and the Al terminal solid solution can contain up to 83.1 wt pct Zn.[46] The presence of large amounts of Zn as a solute in the Al lattice can largely shift the diffraction angles of the Al solid solution. The diffraction pattern of the 5Al-GA coating was identical to that of the GA coating. Both were composed of the δ-$FeZn_{10}$ and Γ-Fe_3Zn_{10} phases formed *via* the Fe-Zn interdiffusion. The SEM/EDS analyses found that the Fe content of the GA and 5Al-GA coatings was 12.43 wt pct and 11.76 wt pct, respectively. This is consistent with the results that both coatings are composed of the δ-$FeZn_{10}$ and Γ-Fe_3Zn_{10} phases.

Figure 4 shows the cross-sectional characterization of the as-coated press hardening steels. The thickness of each coating was reported as the average of ten measurements on three SEM micrographs. The average thickness of both the GI and 5Al-GI coatings was 12 ± 1.5 μm; meanwhile, that of the GA and 5Al-GA coatings was 15 ± 2 μm. The slightly larger thickness of the GA and 5Al-GA coatings compared to the GI and 5Al-GI coatings is due to the Fe-Zn interdiffusion occurring during galvannealing.[24] The element mapping results show that the GI coating was mainly the η-Zn phase and the Al signal was solely detected at the interface between the coating and the steel substrate (Figure 4(a)). Similar result of the formation of a Fe-Al layer as an inhibition layer on commercial GI steel has been well documented in the literature.[23,24,47,48] The GA coating was composed of Zn and Fe, with a slightly higher Fe at the coating/substrate interface. This is consistent with the XRD results showing the presence of Γ-Fe_3Zn_{10} phase as a minor phase in the GA coating (Figure 3). Moreover, the Al content was scanty in the coating and detected predominantly near the surface of the coating. The cross section of the 5Al-GI coating displayed two distinct regions, including oval and lamellar structures. The element mappings further revealed that the oval structure was the primary η-Zn phase and the lamellar structure was the η-Zn and β-Al eutectic structure.[24,46] Moreover, a higher Al intensity was observed at the interface between the coating and substrate, indicating the presence of Fe-Al phases at the interface. Again, the element mapping result of the 5Al-GA coating was similar to those of the GA coating, showing that the constituents of the coating were the δ-$FeZn_{10}$ and Γ-Fe_3Zn_{10} intermetallic phases. However, discrete Fe-Al patches were observed on the surface of the 5Al-GA coating, but not on the GA coating.

B. *Microstructure of the Coating After Austenitization*

To study the microstructural evolution during austenitization, the coated steels were heat treated at 1183 K (910 °C) for 5 minutes. The XRD patterns show that

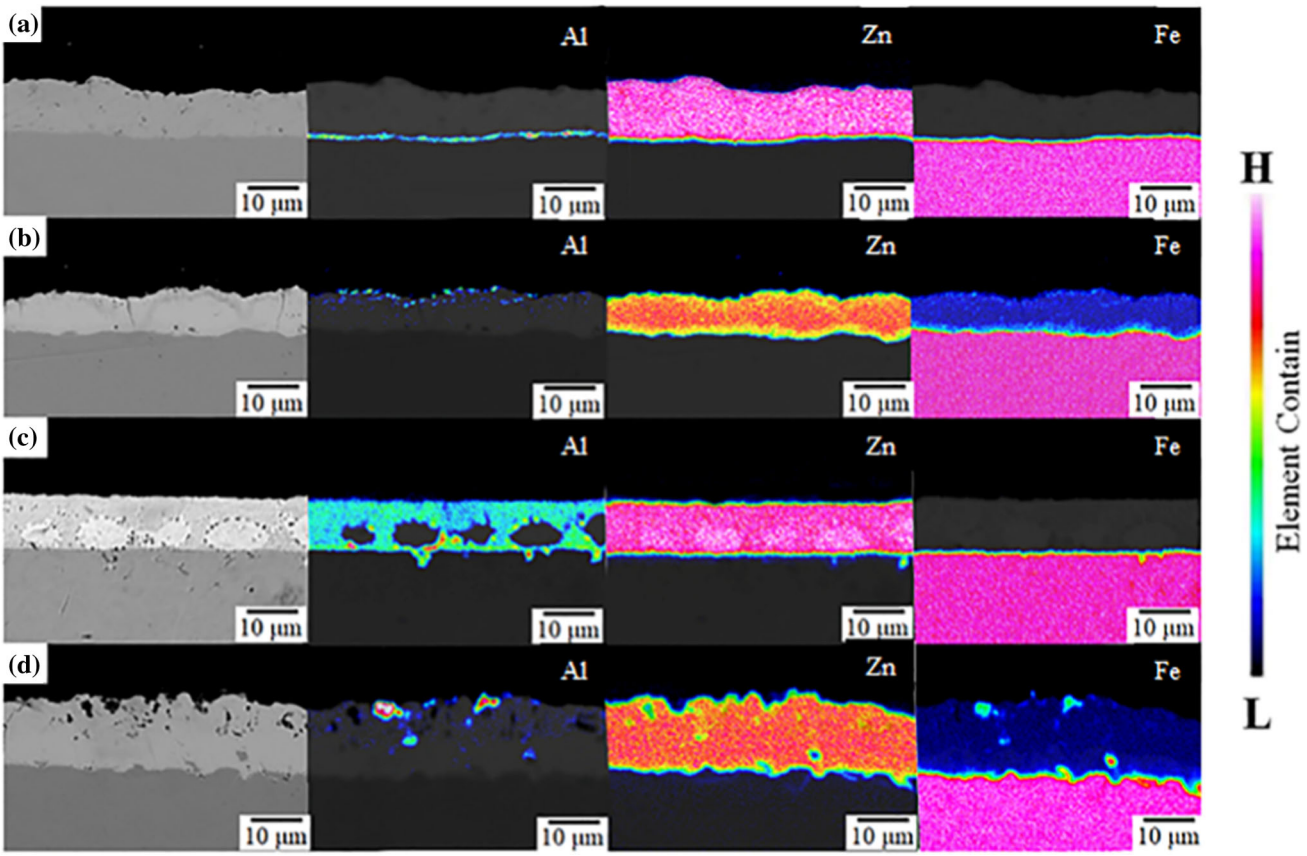

Fig. 4—SEM micrograph and EPMA mapping of the as-coated press hardening steels: (*a*) GI, (*b*) GA, (*c*) 5Al-GI, and (*d*) 5Al-GA.

except the 5Al-GI coating, the GI, GA, and 5Al-GA coatings had suffered severe oxidation, as evident from the obvious peaks of ZnO (Figure 5). Specifically, the austenitized GA steel had the highest relatively intensity of ZnO peaks, followed by the austenitized GI and 5Al-GA steels.

In addition to Zn oxides, both the Zn-containing α-Fe [α-Fe(Zn)] and Γ-Fe_3Zn_{10} phase were present in the alloy layer of the austenitized GI steel, whereas only α-Fe(Zn) was present in that of the austenitized GA steel. The diffraction peaks of the α-Fe(Zn) can be identified as a bcc structure, but shifted to smaller 2θ values compared to those of the α-Fe. The lattice constant of the α-Fe(Zn) was calculated to be approximately 0.2914 nm for the austenitized GA, 5Al-GI, and 5Al-GA steels, as well as 0.2939 nm for the austenitized GI steel, which corresponds to 1.67 and 2.55 pct larger than the lattice constant of the α-Fe. This is consistent with the fact that Zn has an atomic size larger than Fe.[48] The shift of diffraction angles of the α-Fe(Zn) to smaller values was also noticed for austenitized GI 22MnB5 and Zn-Ni-electroplated 22MnB5 steels.[49] Mörtlbaueret *et al.* used *in situ* XRD to characterize the phase evolution of a GI steel during press hardening and found that the Zn-containing α-Fe formed at 1073 K and 1173 K (800 °C and 900 °C) exhibits a bcc structure with a lattice constant of 0.2963 nm.[50] Moreover, the thermal expansion is compensated by the

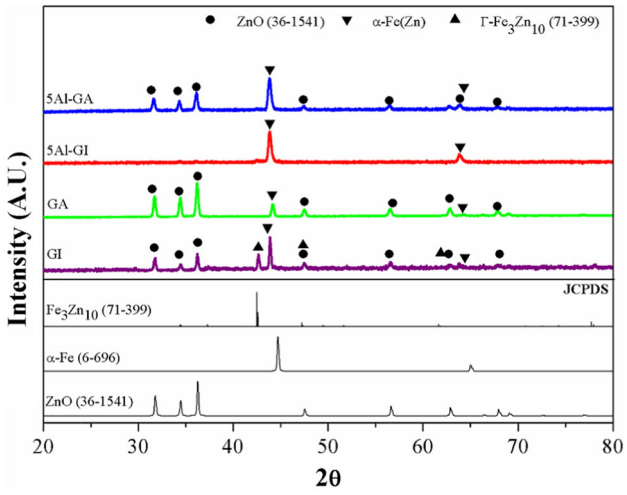

Fig. 5—XRD patterns of the coated press hardening steels after 5 min of austenitization at 1183 K (910 °C).

substitute of Fe by Zn, signifying that up to 46 wt pct Zn can dissolve in α-Fe at 1055 K (782 °C) corresponding to the α-Fe(Zn) + molten Zn peritectic reaction, but the solubility of Zn in α-Fe decreases with increasing temperatures exceeding 1055 K (782 °C).[24] The α-Fe(Zn) in the present study has a Zn content markedly larger than the solubility of the α-Fe(Zn) at room temperature found in the Zn-Fe phase diagram, as will be shown later in Table I. As a result, the α-Fe(Zn) present in the austenitized Zn- and Zn-5Al-coated press hardening steels is metastable and can have a lattice constant larger than the stable counterpart existing in the phase diagram. This is consistent with the literatures showing that the metastable Zn-containing α-Fe prepared by electroplating[51] and ball milling[52] (the Fe—30 at. pct Zn alloy in Reference 52) has a lattice constant larger than 0.2866 nm (the lattice constant of α-Fe at room temperature).

Figure 6 shows the overall cross-sectional microstructure of the various coated steels after austenitization at 1183 K (910 °C) for 5 minutes, illustrating the general morphology of the surface oxide scale. The oxide scale was continuous on the austenitized GA steel; however, that on the austenitized GI steel had broken fragments (Figures 6(a) and (b)). This is consistent with the results made by other researchers.[14,25,26,53] Conversely, insignificant oxidation was observed on the austenitized 5Al-GI steel (Figure 6(c)). A discontinuous oxide layer was observed on the austenitized 5Al-GA steel and was thinner than on the austenitized GA steel, as evident by comparing Figures 6(b) through (d). This indicates that the presence of Al in the Zn coating has positive effect on high-temperature oxidation resistance.

Figure 7 shows the detailed cross-sectional SEM and EPMA characterizations of the coated steels after austenitization. The alloy layer is denoted as the diffusion layer herein to emphasize its formation *via* extensive interdiffusion during austenitization. A continuous oxide layer (presumably ZnO) was observed on the GI and GA steels after austenitization, as marked by the arrows in Figures 7(a) and (b). The oxide layer on the austenitized GA steel was evidently thicker than that on the austenitized GI steel, consistent with the XRD results. Moreover, the former adhered to the underlying diffusion layer more completely than the latter, as evident from the presence of gaps marked by the double arrows in Figure 7(a). Instead of a continuous oxide layer, patches of particles were observed on the austenitized 5Al-GA steel. EPMA mapping further revealed

Table I. Thickness and EPMA/WDS Analysis of the Diffusion Layer on the Coated Press Hardening Steels After Austenitization

Sample	Diffusion Layer Thickness (μm)	Element Content (Weight Percent)			Phase
		Zn	Al	Fe	
GI	20.8 ± 1.2	70.40 ± 0.15	0.15 ± 0.03	29.45 ± 0.20	Γ-Fe_3Zn_{10}
		34.01 ± 0.17	0.08 ± 0.01	65.91 ± 0.25	α-Fe(Zn)
GA	17.0 ± 1.5	29.18 ± 0.13	0.03 ± 0.01	70.81 ± 0.10	α-Fe(Zn)
5Al-GI	27.7 ± 1.1	29.90 ± 0.10	0.68 ± 0.12	69.42 ± 0.22	α-Fe(Zn)
5Al-GA	17.2 ± 1.8	29.42 ± 0.16	0.53 ± 0.05	70.05 ± 0.25	α-Fe(Zn)

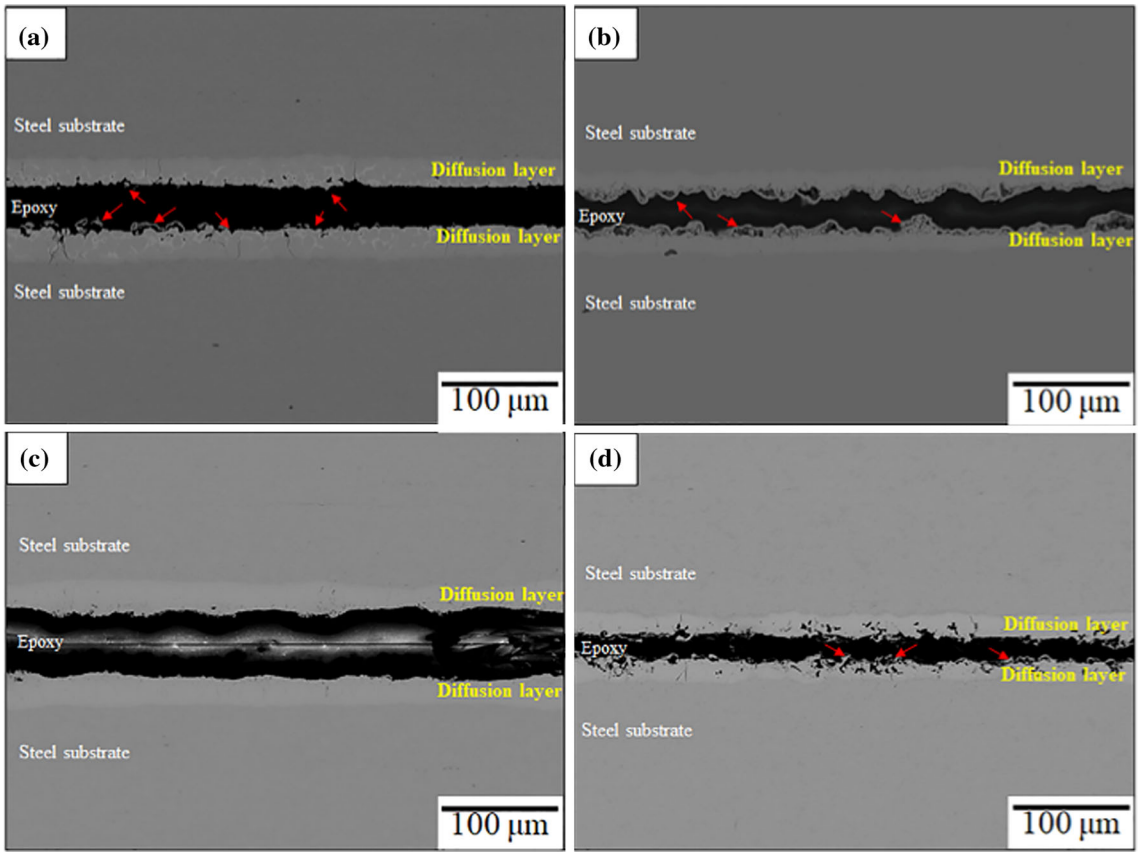

Fig. 6—Cross-sectional SEM micrograph at low magnifications of the coated press hardening steel after austenitization at 1183 K (910 °C) for 5 min: (*a*) GI, (*b*) GA, (*c*) 5Al-GI, and (*d*) 5Al-GA. Note the red arrows indicate the oxide layer.

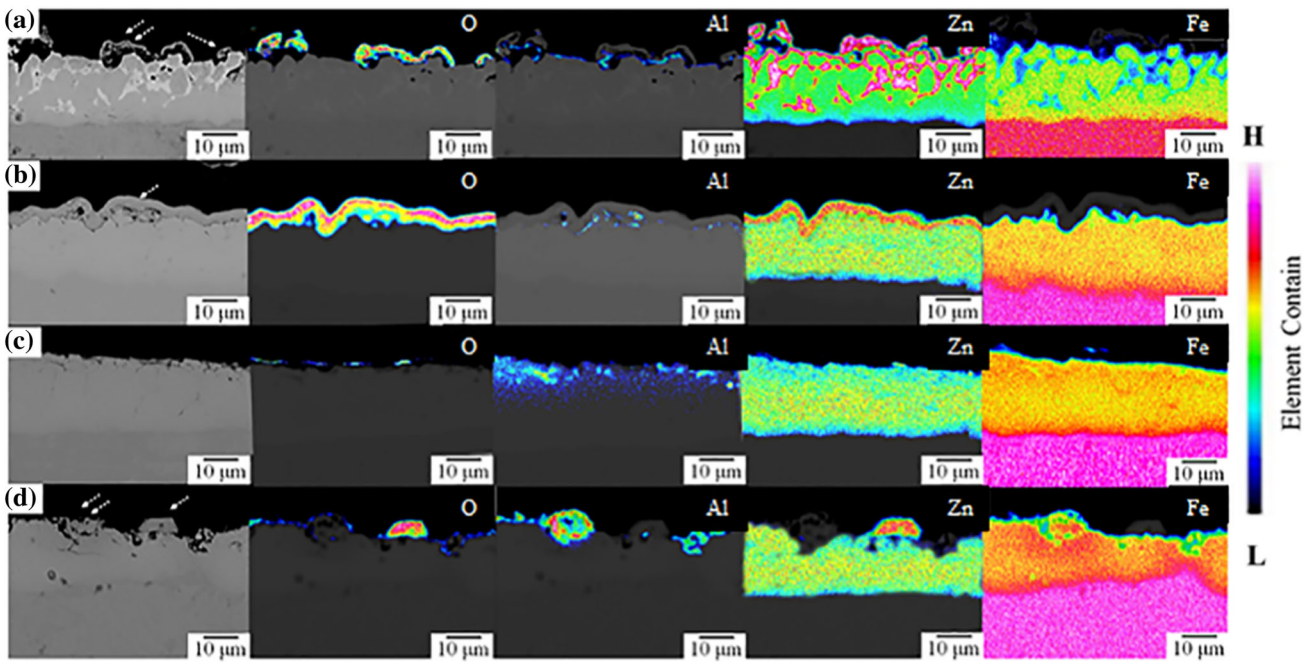

Fig. 7—SEM micrograph and EPMA mapping of the coated press hardening steels after 5 min of heating at 1183 K (910 °C): (*a*) GI, (*b*) GA, (*c*) 5Al-GI, and (*d*) 5Al-GA.

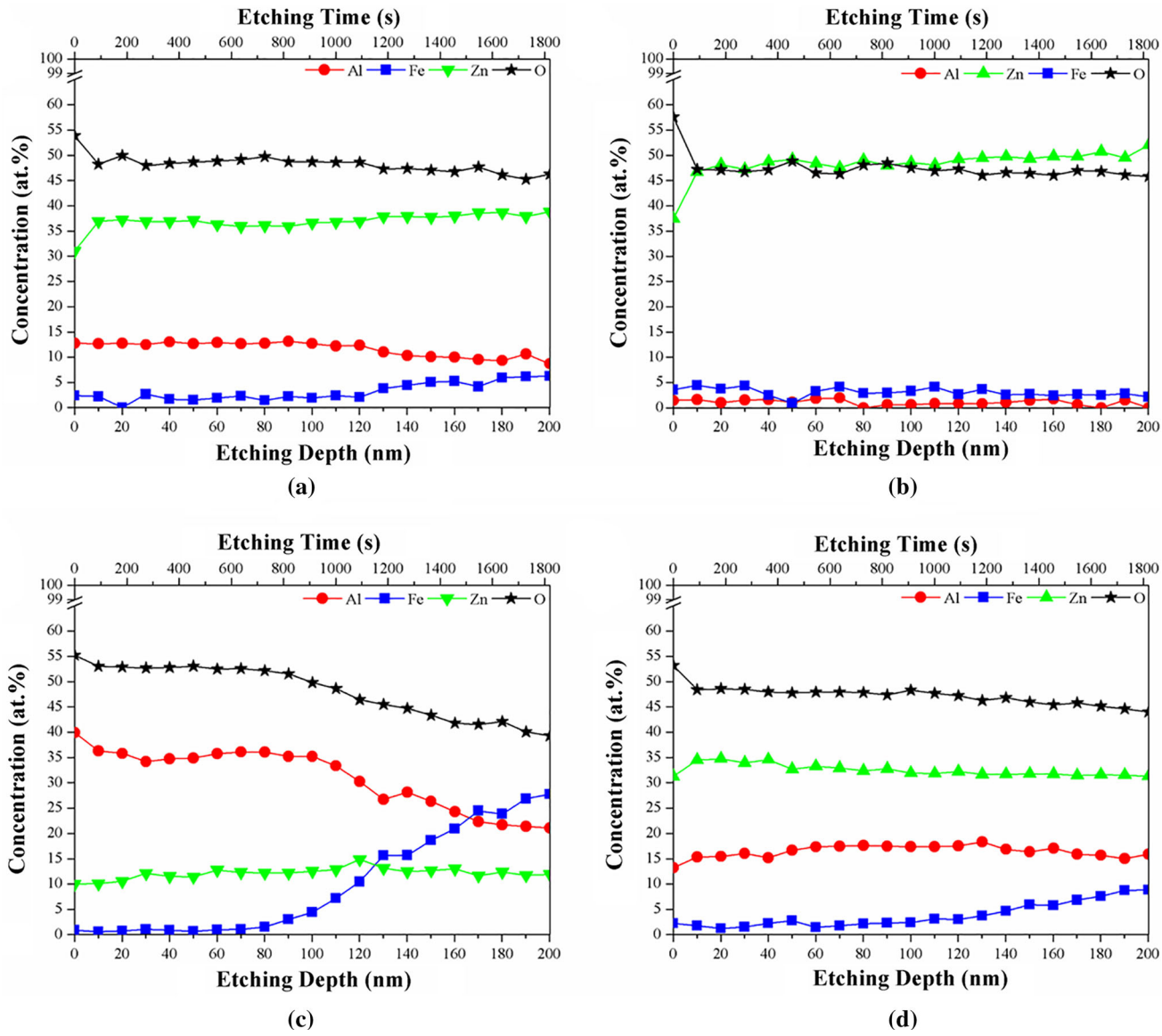

Fig. 8—The XPS depth profile of the coated press hardening steels after 5 min of heating at 1183 K (910 °C): (*a*) GI, (*b*) GA, (*c*) 5Al-GI, and (*d*) 5Al-GA.

the presence of ZnO patch (marked as the arrow in Figure 7(d)), Fe-Al particles covering with an Al oxide layer (marked as the double arrows in Figure 7(d)), and a discontinuous, thin Al oxide layer. Table I summarizes the thickness and WDS composition of the individual Fe-Zn phase in the diffusion layer. It can be seen from Table I that (1) the thickness of the diffusion layer increased with the presence of Al and the absence of Fe in the coating prior to austenitization; (2) the amount of Zn in the diffusion layer, which can be approximately estimated as the average Zn content multiplying the thickness of the diffusion layer, also increased with the presence of Al and the absence of Fe in the coating prior to austenitization; (3) the Al was absent in the austenitized GI- and GA-coated steels; (4) the Al in the diffusion layer was scant compared to the coating before austenitization. The diffusion layer of the austenitized GI steel contained around 70 wt pct Zn in Γ-Fe_3Zn_{10} phase, and 34 wt pct Zn in α-Fe(Zn) in consistence with the coexistence of the α-Fe(Zn) and Γ-Fe_3Zn_{10} (the XRD results in Figure 5). Moreover, the presence of 5 wt pct Al in the coating markedly reduced the extent of oxidation; thereby, more α-Fe(Zn) was retained after austenitization.

XPS was further employed to study the composition of the surface layer down to a depth of approximately 200 nm of the coated steel after austenitization (Figure 8). The 200-nm-thick surface layer of the austenitized GI and 5Al-GA steels comprised, in the decreasing order, ZnO, Al_2O_3, and Fe_3O_4 (Figures 8(a) and (d)). The surface layer of the austenitized GA steel was mainly composed of ZnO (Figure 8(b)). Conversely, the austenitized 5Al-GI steel consisted of Al_2O_3 as the major phase and ZnO as a minor phase. Moreover, at 100 nm down to the surface of the austenitized 5Al-GI steel, a rapid increase in the Fe content was detected.

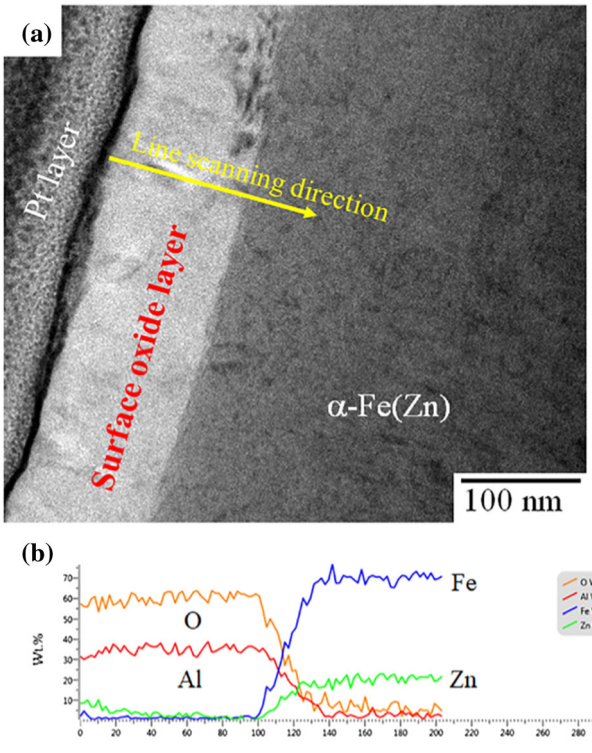

Fig. 9—(*a*) A cross-sectional TEM micrograph and (*b*) the line scanning results marked as the red arrow in (a) of the 5Al-GI steel after 5 min of austenitization at 1183 K (910 °C).

This indicates that the α-Fe(Zn) was present at around 100 nm down the surface. As a result, the oxide layer on the austenitized 5Al-GI steel was relatively thin, which is in good consistence with the results of XRD, SEM, and EPMA. A close investigation of the results in Figure 8 shows that (1) the presence of Al in the coating contributed to the formation of Al_2O_3 in the surface layer; (2) the presence of Fe in the coating resulting from galvannealing reduced the amounts of Al_2O_3 in the surface layer; and (3) 5 wt pct Al in the Zn coating without Fe was sufficient to ameliorate the severe oxidation of the coating *via* the formation of a thin, continuous Al_2O_3 layer.

Figure 9 shows the cross-sectional TEM characterization of the 5Al-GI steel after austenitization. The surface oxide layer was approximately 100 nm thick (Figure 9(a)). The EDS line scan across the surface oxide layer further confirmed that the oxide layer was mainly composed of Al_2O_3 with few ZnO (Figure 9(b)). Moreover, the alloy layer right beneath the Al_2O_3 layer was the α-Fe(Zn). Both the TEM and XPS results confirm the presence of approximately 100-nm-thick Al_2O_3 with small amounts of ZnO on the surface of austenitized 5Al-GI steel, signifying the effectiveness in preventing oxidation during austenitization. Oxide scales are commonly seen in hot-stamped parts made of bare press hardening steels and those with commercial GI and GA coatings.[14,17] Thick oxide scales generally deteriorate the resistance spot weldability and thus should be removed using sandblasting.[14] The thin oxide layer on the austenitized 5Al-GI steel is thus beneficial in industrial implementations in terms of the necessary surface pretreatment prior to resistance spot welding.[28,29,54]

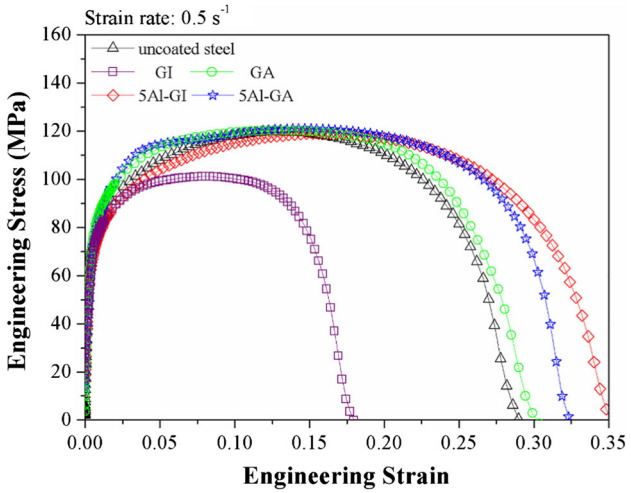

Fig. 10—Stress–strain curves of the bare and coated press hardening steels tested at 1183 K (910 °C).

C. *High-Temperature Tensile Test*

Figure 10 shows the stress–strain curves of bare press hardening steel, and GI, GA, 5Al-GI, as well as 5Al-GA press hardening steels tested at 1183 K (910 °C) after a total heating time of 5 minutes. The ultimate tensile strength (UTS) and elongation of the bare press hardening steel were approximately 120 MPa and 0.3, respectively. An obvious decrease in both the UTS and elongation was observed for the GI steel. In contrast, the GA, 5Al-GI, and 5Al-GA press hardening steels had comparable UTS and slightly larger elongation compared to the bare press hardening steel. As a result, the GI steel was prone to the LME, the other three coated steels were not.

D. *Electrochemical Tests*

Sacrificial protection of Zn-based coating on steel is generally evaluated by the difference in the corrosion potential of the coating and the steel substrate. Chemical stripping test[45,54–56] was thus used to measure the potential difference between the coating and the substrate in 4 wt pct HCl solution at 298 K (25 °C),[45] as shown in Figures 11(a) and (b) for the coated press hardening steel before and after austenitization, respectively. Following a sharp increase in the potential upon immersion, the potential of both the GI and 5Al-GI steels reached a plateau at − 1.06 V_{SCE}, which is a characteristic of the chemical reactivity of Zn in HCl solution. The plateau potential lasted for 400 and 2200 seconds for the GI and 5Al-GI steels, respectively. This is consistent with the results commonly seen in the literature showing that the presence of Al in Zn coatings enhances the corrosion resistance of the coating.[36–38] The potential then exhibited a sharp increase and reached a second plateau at − 0.5 V_{SCE} associated with

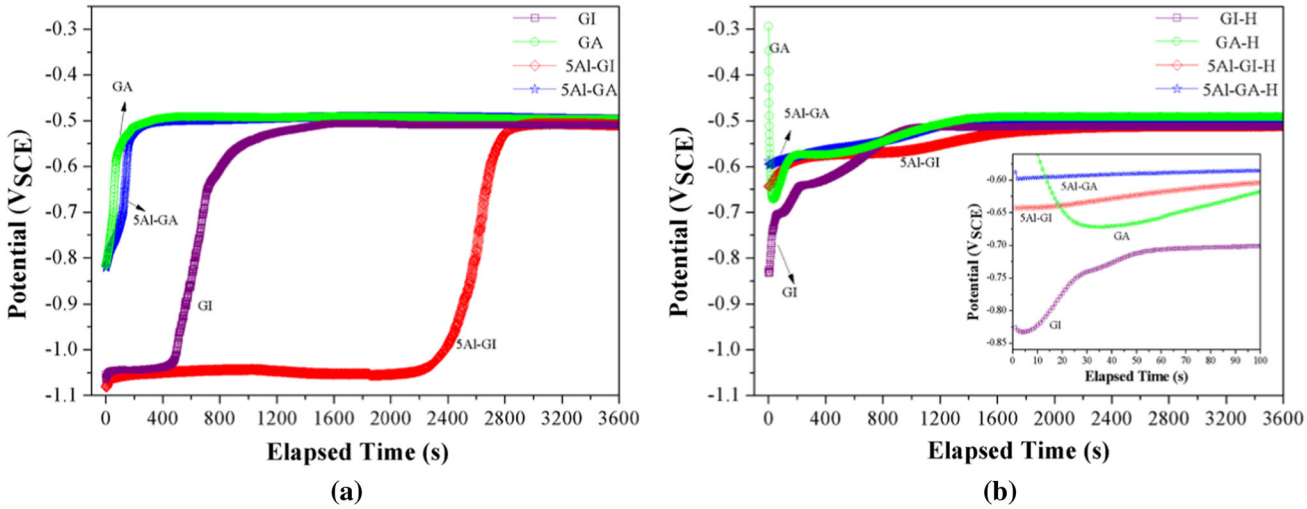

Fig. 11—Potential evolution of (*a*) the as-coated press hardening steels and (*b*) the coated press hardening steels after austenitization measured in 4 wt pct HCl solution at 298 K (25 °C).

the steel substrate when the coating had been completely removed. As for the GA and 5Al-GA steels, the potential rose rapidly during the early stages of immersion and soon reached the plateau potential of the steel substrate compared to the GI and 5Al-GI steels. The elapsed time reaching the exposure of the steel substrate increased in the order of GA, 5Al-GA, GI, and 5Al-GI steels, indicating that (1) the presence of Al in the coating is beneficial for the corrosion resistance in HCl solution; (2) the alloying with Fe deteriorates the corrosion resistance in HCl solution; (3) the beneficial effect of Al is largely offset by the presence of Fe in the Zn-based coatings.

After austenitization, the potential of the coated steels also evolved from a minimum value upon immersion in 4 wt pct HCl solution at 298 K (25 °C) except for the austenitized GA steel. The potential of the austenitized GA steel declined sharply upon immersion, reached a lowest point, and rapidly rose again. This initial decrease in the potential is apparently due to the removal of surface oxides, which agrees with the result that the austenitized GA steel had a thickest oxide layer among the coated steels studied (Figures 7 and 8). Moreover, the minimum potential increased (shifted in the positive direction) in order the of GI, GA, 5Al-GI, and 5Al-GA steels, as shown in the inset in Figure 11(b). Following the minimum potential, the potential increased when chemically more active elements were oxidized and removed first. Finally, the potential reached the plateau potential of the steel substrate. The potential of the austenitized GI steel evolved from -0.83 V_{SCE}, which is similar to that of the as-coated GA and 5Al-GA steels (Figures 11(a) and (b)). Because the coating of the as-coated GA and 5Al-GA steels consisted of the δ-$FeZn_{10}$ phase as the major overlay, the δ phase was likely to be present on the surface of the austenitized GI steel. The formation of the Γ-Fe_3Zn_{10} phase and δ-$FeZn_{10}$ phase proceeds *via* a peritectic reaction at 782 °C and 665 °C, respectively.[24] The peritectic reaction of α-Fe(Zn) + Zn(Fe) melt to form the Γ-Fe_3Zn_{10} phase did not complete during rapid cooling for press hardening steel. At lower temperatures, the remnant Zn(Fe) melt can react with the Γ-Fe_3Zn_{10} phase to form the δ-$FeZn_{10}$ phase.[27] This agrees with the corrosion potential of the Γ-Fe_3Zn_{10} and δ-$FeZn_{10}$ phases measured in 100 g L^{-1} $ZnSO_4$ and 200 g L^{-1} NaCl solution, *i.e.*, -0.77 V_{SCE} and -0.82 V_{SCE}, respectively.[54] Moreover, up to the intermediate stages of immersion, the potential of the austenitized GI steel was more negative to that of the other three austenitized coated steels. This correlates to the existence of the Γ-Fe_3Zn_{10} phase in between the α-Fe(Zn) grains. As a result, the chemical stripping can be a quick, feasible method to evaluate whether or not the Γ-Fe_3Zn_{10} phase coexists with the α-Fe(Zn). This is important because the presence of Γ-Fe_3Zn_{10} phase is indicative of the existence of liquid Zn(Fe) phase during hot stamping, which is one of the prerequisites causing the LME.[14,30–33,57,58] Nevertheless, the Γ-Fe_3Zn_{10} and δ-$FeZn_{10}$ phases have corrosion potentials negative to the steel substrate, which is essential for the cathodic protection afforded by the diffusion layer.

A close comparison of the curves in Figure 11(b) shows that (1) before reaching the plateau potential of the steel substrate, the presence of Al in the coating shifted the potential along the positive direction and (2) the alloying with Fe in the coating prior to austenitization also shifted the potential along the positive direction and slightly elevated the plateau potential. A comparison between Figures 11(a) and (b) further shows that (1) the austenitization treatment markedly reduced the elapsed time to reach the plateau potential; (2) the austenitization treatment reduced the difference in the potential *vs* time curves of the various coated steels.

The corrosion resistance of the various coated steels was further studied using the potentiodynamic polarization method in 0.1 M NaCl solution at 298 K (25 °C) (Figure 12 and Table II). All the coated steels had E_{corr} more negative than the bare steel, indicating the

cathodic protection of the Zn and 5Al-Zn coatings. For the GI and GA steels, alloying with Fe retarded the anodic kinetics, but had a slight effect on the cathodic kinetics (Figure 12(a)). As a result, the GA steel had a nobler E_{corr} than the GI steel. A similar trend was also observed for the comparison of 5Al-GI *vs* 5Al-GA steels. In contrast, the presence of Al in the coating inhibited the cathodic kinetics, but hardly influenced the anodic kinetics, leading to a negative shift in the E_{corr}. This is consistent with the fact that the corrosion products of Zn-Al coating are more effective in retarding the diffusion of reaction species of the test solution (1 M NaCl solution), but is not effective against the dissolution in Cl^--containing solutions during anodic polarization.[59–61]

As for the coated steels after austenitization, the austenitized GA steel had the E_{corr} comparable to that of the bare steel, but its anodic and cathodic kinetics were slower compared to the bare steel. This can be associated with the relatively thick, compact oxide layer present on the surface of the austenitized GA steel. The polarization curves were similar for the other three coated steels and the cathodic kinetics increased in the order of 5Al-GI, 5Al-GA, and GI steels. It is likely that the presence of a thin, compact Al_2O_3/ZnO(minor) layer retards the cathodic reaction, which is known to be the reduction of oxygen in non-deaerated NaCl solution.[62,63] Finally, a scrutiny of Table II reveals that (1) the austenitization treatment ennobled the E_{corr} regardless of the coating composition; (2) the cathodic kinetics were largely governed by the presence of the compact oxide layer; (3) the anodic kinetics were primarily related to the composition of the coating or the diffusion layer.

Table II. Potentiodynamic Polarization Results of the Coated Press Hardening Steels

Before Austenitization		
Sample	E_{corr} (mV_{SCE})	I_{corr} ($\mu A/cm^2$)
Press Hardening Steel	− 698	3.07
GI	− 1053	7.92
GA	− 880	8.08
5Al-GI	− 1158	3.52
5Al-GA	− 949	2.09
After Austenitization		
Sample	E_{corr} (mV_{SCE})	I_{corr} ($\mu A/cm^2$)
Press Hardening Steel	− 630	11.39
GI	− 730	14.28
GA	− 629	13.78
5Al-GI	− 733	3.05
5Al-GA	− 725	5.43

IV. DISCUSSION

The high-regarded design philosophy for the protective coating on press hardening steel is that the coating should offer resistance against high-temperature oxidation and decarburization while it does not cause the LME during press forming. The resulting alloy layer (diffusion layer) after press hardening should also provide sufficient corrosion protection, including the barrier and sacrificial protections. Furthermore, the surface scale cannot impair the resistance spot weldability of the press hardened steel parts. Under this design paradigm, the Al-Si coating meets most of the requirements except the sacrificial corrosion protection. Zn-based coating has advantages over the Al-Si coating due to the sacrificial protection afforded by the chemically active Zn. However, the Zn-based coating has oxidation resistance markedly inferior to the Al-Si coating and tends to cause the LME due to the presence of Zn(Fe) melt that subsequently solidifies to form Fe-Zn intermetallic phases (mainly the Γ-Fe_3Zn_{10}

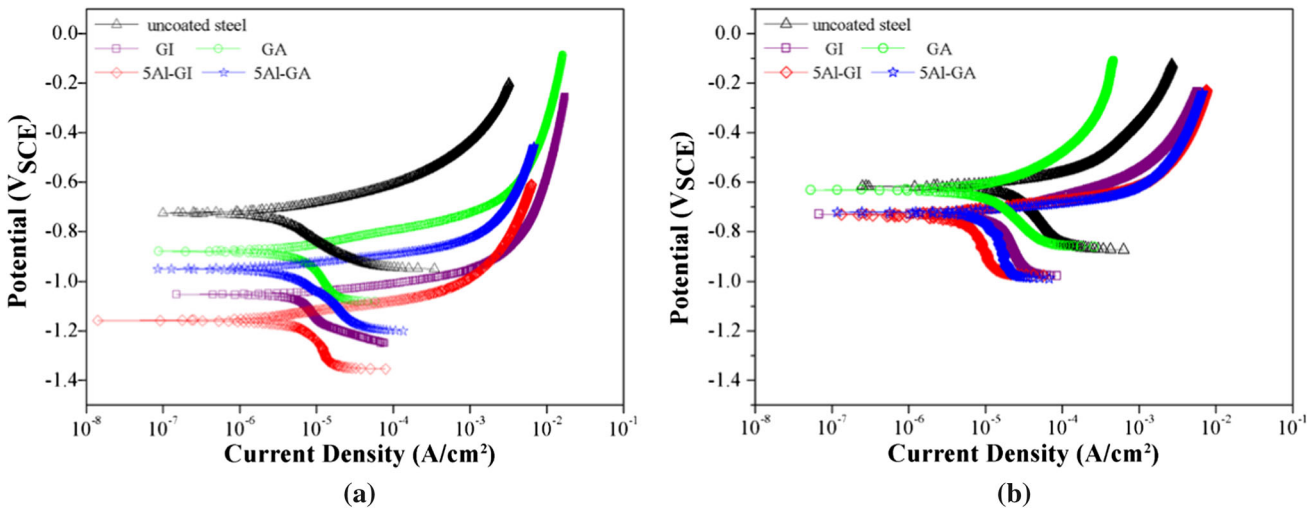

Fig. 12—Polarization curve of (*a*) the as-coated press hardening steels and (*b*) the coated press hardening steels after austenitization measured in 0.1 M NaCl solution at 298 K (25 °C).

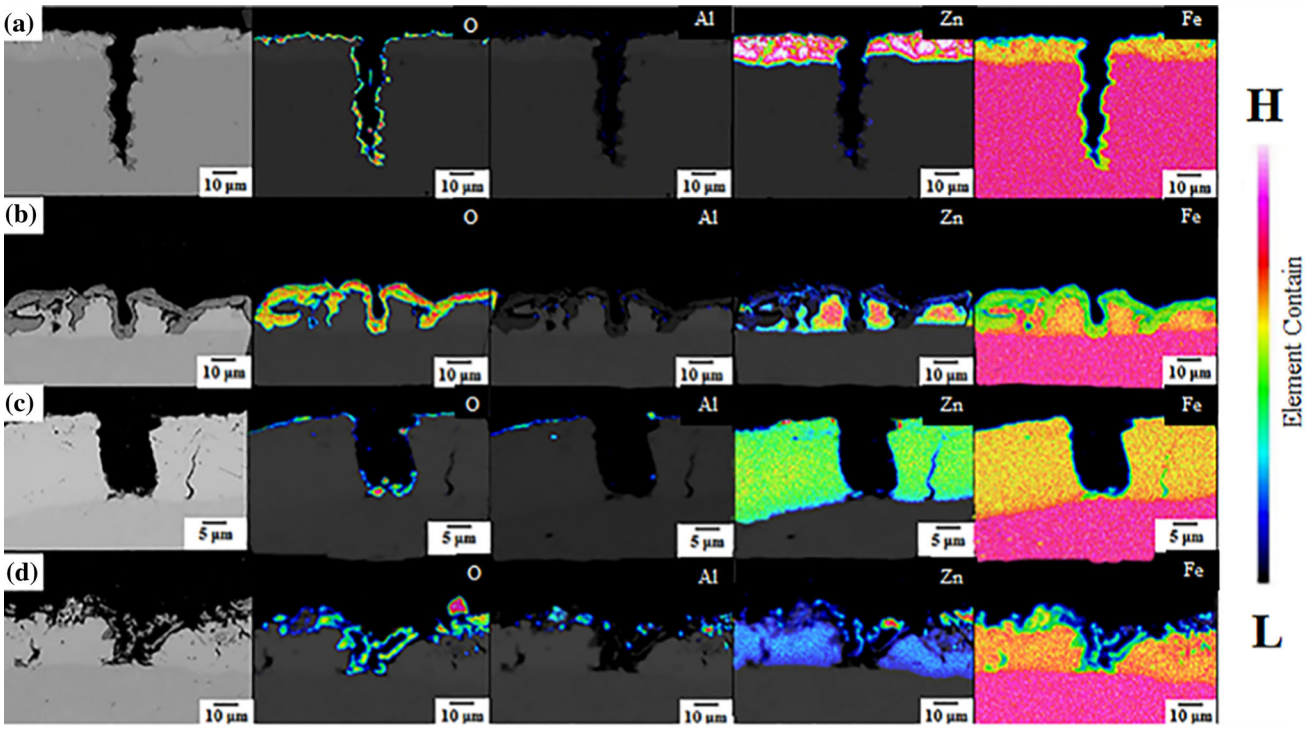

Fig. 13—Cross-sectional SEM micrograph and related EPMA/WDS element distributions of the different coated steels (*a*) GI, (*b*) GA, (*c*) 5Al-GI, and (*d*) 5Al-GA after 5 min of isothermal holding at 1183 K (910 °C) and subsequent tensile deformation. Note: Fig. 12(c) is presented at a higher magnification to show the presence of a thin Al_2O_3 layer.

phase). The applicability of Zn-based coatings is thus dependent on how to balance the overall performance of the coating *via* the composition design and process control. Compared to the GI coating, the presence of 5 wt pct Al in the Zn coating on press hardening steel influences the phase evolution during austenitization, which, in turn, determines the properties of the coating, as discussed below.

A. *Phase Evolution*

5 wt pct Al in the Zn bath is effective to inhibit the formation of the Fe-Zn intermetallic phases during hot dipping. However, the 5 wt pct Al has little effect on the transformation of the Fe-Al inhibition layer to the Fe-Zn intermetallic phases during subsequent galvannealing and austenitization. This indicates that the reaction between molten Zn and steel substrate proceeds rapidly in a thin molten Zn-5 wt pct Al layer. This is different from the 55 wt pct Al-Zn coating on 22MnB5 steel in which a Fe-Al diffusion layer forms after austenitization.[40,41]

A possible transformation path of the 5 wt pct Al-Zn coating on press hardening steel during austenitization is thus proposed. During the rapid heating up to the austenitization temperature, the 5 wt pct Al-Zn coating melts down before sufficient Fe diffuses to the coating. The Al in the melt diffuses down the chemical potential, largely to the surface to form Al_2O_3, and, to less extents, to the interface to support the growth of the Fe-Al phase. Because the Fe-Al phases are absent after austenitization, the Fe-Al phase transforms to the Fe-Zn phases following the reaction paths commonly seen in commercial GA coatings.[24]

It is apparent that most of the Al diffuses to the surface to form Al_2O_3; thereby, the reduction in Gibbs free energy *via* the Al_2O_3 formation prevails in the 5 wt pct Al-Zn melt during austenitization. According to the high-temperature oxidation theory of alloys,[65] the spontaneity of oxidation is governed by the Gibbs formation energy of oxides and the rate of oxidation is determined by diffusion of reacting species. For the Zn-based alloy coatings of this present study, Fe, Al, and Zn are all prone to oxidation during austenitization under ambient atmosphere. The Gibbs free energy of formation for ZnO, Al_2O_3, and Fe_3O_4 at 1183 K (910 °C) is − 217, − 872, and − 677 kJ mol^{-1}, respectively.[66] As a result, both Al and Fe are more susceptible to oxidation than Zn. Moreover, Al_2O_3 is more protective against oxidation than Fe_3O_4 because the Pilling Bedworth ratio of Al and Fe is 1.29 and 2.1, respectively.[65] Therefore, the hot-dip galvannealed coating suffered larger extents of oxidation than the galvanized coating regardless of the Al content in the coating (Figures 6 and 7). The presence of Fe in the coating is thus detrimental to the high-temperature oxidation resistance of Zn(Al)-based coatings on steels. This is consistent with the studies showing that unlike the compact Al_2O_3 layer, Fe oxide scale is porous and fails to provide effective barrier for further oxidation.[14,17] Finally, the presence of compact Al_2O_3 layer is of great importance for suppressing the vaporization

of Zn and the intensive formation of ZnO. Consequently, the presence of 5 wt pct Al contributes to the reduction in the thickness of oxide scales, which is essential to ensure the resistance spot weldability.

B. *The Liquid Metal Embrittlement Behavior*

The typical difference between the coated press hardening steel suffering the LME from that not suffering the LME is the presence of obvious Γ-Fe_3Zn_{10} phase after press hardening. This LME phenomenon and mechanism on Zn-coated steels has been studied in detail.[14,30–33] Compared to the GI press hardening steel, the presence of 5 wt pct Al in the coating reduces the amount of the Γ-Fe_3Zn_{10} phase after press hardening. The molten Zn(Fe) in the steel is thus not sufficient to wet the grain boundaries of the α-Fe(Zn); thereby, the LME problem is ameliorated. This is further confirmed using the EPMA characterization on the cross sections of the coated press hardening steels after high-temperature tensile test (Figure 13). Cracks with sharp tips propagated down to the steel substrate for the GI steel (Figure 13(a)). In contrast, crack propagation was confined in the diffusion layer for the GA, 5Al-GI, and 5Al-GA steels (Figures 13(b) through (d)). These cracks exhibited a typical U shape, indicative of the absence in wetting of the α grain boundaries by molten Zn(Fe). The beneficial effect of the presence of Al in Zn-1.6 wt pct Mg coating on LME for press hardening steel is also noted by De Cooman *et al.*[67] However, in this present study it is not immediately clear as why the amount of the Γ-Fe_3Zn_{10} phase is reduced when 5 wt pct Al is present. Approximately 0.6 wt pct Al dissolves in the diffusion layer of the 5Al-GI steel in contrast to the GI steel in which the content of Al is below the detectable limit of the WDS (Table I). Further studies are needed to elucidate the major role of the Al in Zn(Fe) melt in the wetting behavior along the austenite grain boundaries during austenitization, which is considered to be a crucial mechanism by which Al suppresses the Zn penetration.[67]

C. *Corrosion Protection*

Zn-based coating is known for barrier protection and sacrificial/cathodic protection over steels. All the Fe-Zn intermetallic phases and the α-Fe(Zn) have corrosion potentials negative to the press hardening steel (Figure 12). As a result, the as-coated coating layer and the diffusion layer all can provide cathodic protection over the steel substrate.[17] However, the effective sacrificial protection on deep-drawing quality special-killed steel (a type of low-carbon steel) has been measured to be an imposed potential of − 0.725 V_{SCE}.[64] Moreover, the protection in distance increases with the difference in the corrosion potential of the coating and the steel substrate. Consequently, the austenitized GI steel has the best cathodic protection capacity among the four coated press hardening steels studied (Figure 11(b)), which is attributed to the presence of Γ-Fe_3Zn_{10}.[25,26,30,31]

Galvannealing after hot-dip galvanizing increases the Fe content of Zn coatings such as GA and 5Al-GA coatings. As a result, both GA and 5Al-GA coatings have E_{corr} higher than GI and 5Al-GI counterparts. It has been shown previously that alloying Zn coating with Fe ennobles the E_{corr} owing to the standard reduction potential of Fe (− 0.440 V) is nobler than that of Zn (− 0.763 V) and Al (− 1.662 V).[49] After the austenitization heat treatment, more Fe diffuse to the Zn coating, further increasing the E_{corr} of Zn(Al)-coated steels. For the I_{corr}, the austenitization treatment results in an increase in the I_{corr}, except the austenitized 5Al-GI steel (Table II). Furthermore, passivation behaviors were not observed in both the austenitized 5Al-GI and 5Al-GA-coated steels. Lee *et al.*[40,41] and Lin *et al.*[68,69] found that the presence of Fe-Al intermetallic phases in the austenitized 55 wt pct Al-Zn coating and hot-dip galvanized 5 wt pct Al-Zn and 55 wt pct Al-Zn coatings resulted in passivation in 5 wt pct NaCl solution. In this study, both the austenitized 5Al-GI and 5Al-GA alloy layer mainly comprise α-Fe(Zn); thereby, they do not exhibit passivation in 0.1 M NaCl solution. Therefore, for short-term corrosion resistance tested in 0.1 M NaCl solution, the austenitized 5Al-GI press hardening steel outperforms the other three steels in terms of the smallest I_{corr}. The retarded cathodic kinetics in the austenitized 5Al-GI press hardening steel indicates that the presence of 5 wt pct Al in the coating can be beneficial for the barrier corrosion protection of the press hardening steel in 0.1 M NaCl solution.[70,71]

D. *The Overall Performance*

Alloying the Zn coating with Fe or Al is beneficial for reducing the LME susceptibility. However, pre-heating, like galvannealing, to promote the Fe-Zn interdiffusion causes severe oxidation during subsequent austenitization. Conversely, the addition of 5 wt pct Al in the molten Zn bath is effective to reduce oxidation during austenitization. This ensures the resistance spot weldability of the press hardened steel parts. Moreover, the austenitized 5Al-GI press hardening steel has slower cathodic kinetics than the austenitized GI press hardening steel. However, the austenitized GI press hardening steel tends to outperform in terms of cathodic protection.

In conclusion, to design effective Zn-based coating for hot stamping application, the key point is the regulation of the Al composition in Zn bath. The ideal coating composition is that the initial coating has adequate Al so that a thin, compact Al_2O_3 layer can form on the surface. Meanwhile, the presence of Al together with proper austenitization treatments can regulate the Fe/Zn interdiffusion to modulate the volume fraction of molten Zn(Fe) in the α-Fe(Zn) to avoid the LME, yet still reserve sufficient Zn content (mainly Γ-Fe_3Zn_{10} phase and perhaps few δ-$FeZn_{10}$ phase) to act as cathodic protection.

V. CONCLUSIONS

Phase evolution of GI, GA, 5Al-GI, and 5Al-GA-coated press hardening steels during austenitization was studied. The influence of the resultant phase constituents and microstructure of the diffusion layer on the properties of steels was detailed. The key findings are summarized as follows:

1. Both the GA and 5Al-GA coatings consist of the δ-$FeZn_{10}$ and Γ-Fe_3Zn_{10} phases, signifying that the presence of 5 wt pct Al in the Zn bath has little effect on the phase evolution of the Zn coating during subsequent galvannealing at 500 °C for 25 seconds.
2. The diffusion layer resulting from austenitization is mainly composed of the α-Fe(Zn) regardless of the presence of 5 wt pct Al in the Zn coating prior to austenitization. Moreover, the XRD diffraction peaks of the Γ-Fe_3Zn_{10} phase were observed in the austenitized GI steel only.
3. A loose ZnO scale was observed on the austenitized GI and GA steel. In contrast, a 100-nm-thick Al_2O_3 layer was observed on top of the diffusion layer of the austenitized 5Al-GI steel. As a result, the presence of 5 wt pct Al in the coating markedly suppresses the oxidation of the coating during austenitization *via* the formation of a thin, continuous Al_2O_3 layer.
4. The austenitized GA steel suffers oxidation more severely than the austenitized GI steel. Similar trend is also noticed for the austenitized 5Al-GA steel and 5Al-GI steels. Pre-alloying the Zn coating with Fe *via* galvannealing is thus detrimental to the high-temperature oxidation resistance of the coating regardless of the Al content of the coating.
5. The LME was observed in the austenitized GI steel, but not in the austenitized GA, 5Al-GI, and 5Al-GA steels. The Γ-Fe_3Zn_{10} phase present in the austenitized GI steel can cause the LME as it is present as molten Zn(Fe) during austenitization. Moreover, the electrochemical stripping test in 4 wt pct HCl solution is able to detect whether or not the presence of the Γ-Fe_3Zn_{10} phase in the austenitized Zn- and 5Al-Zn-coated press hardening steels.
6. The electrochemical stripping of the coated steels in 4 wt pct HCl solution reveals that the presence of Al and the absence of Fe enhances the corrosion resistance of the as-coated press hardening steels in 4 wt pct HCl. Moreover, the 5Al-GI and 5Al-GA coatings have smaller I_{corr} tested in 0.1 M NaCl solution than their GI and GA counterparts.
7. The austenitized GI press hardening steel has more negative potentials during stripping in 4 wt pct HCl solution, which correlates to the presence of the Γ-Fe_3Zn_{10} in the diffusion layer.
8. The presence of 5 wt pct Al in the Zn coating is beneficial for the overall properties of the austenitized coated press hardening steels, including suppression in oxidation and LME during hot press forming, as well as reduction in I_{corr} in 0.1 M NaCl solution.

ACKNOWLEDGMENT

The authors are grateful to the Ministry of Science and Technology, Taiwan, and China Steel Corporation, Kaohsiung, Taiwan, for their financial supports under Grant MOST 104-2622-8-006-001.

REFERENCE

1. R. Kuziak, R. Kawalla, and S. Waengler: *Arch. Civil Mech. Eng.*, 2008, vol. 8, pp. 103–17.
2. O. Bouaziz, H. Zurob, and M. Huang: *Steel Res. Int.*, 2013, vol. 84, pp. 937–47.
3. J. Galan Lopez, L. Samek, P. Verleysen, K. Verbeken, and Y. Houbaert: *Rev. Metall.*, 2012, vol. 48, pp. 118–31.
4. O. Kwon, K.Y. Lee, G.S. Kim, and K.G. Chin: *Mater. Sci. Forum.*, 2010, vol. 638, pp. 136–41.
5. N. Abedrabbo, R. Mayer, A. Thompson, C. Salisbury, M. Worswick, and I. Van Riemsdijk: *Int. J. Impact Eng.*, 2009, vol. 36, pp. 1044–57.
6. W. Gan, S. Babu, N. Kapustka, and R.H. Wagoner: *Metall. Mater. Trans. A*, 2006, vol. 37A, pp. 3221–31.
7. J. Lin, F. Li, J. Min, J. Jin, H. Gu, Y. Liu, W. Zhang, H. Zhan, Y. Ji, and L. Li: Advanced High Strength Steel and Press Hardening. *Proc. 2nd Int. Conf.*, Changsha, China, 2016, pp. 3–7.
8. M. Geiger, M. Merklein, and C. Hoff: *Adv. Mater. Res.*, 2005, vols. 6–8, pp. 795–804.
9. J.F. Tu, Y.T. Pan, C.Y. Huang, and S.H. Hsieh: *China Steel Tech. Rep.*, 2009, vol. 22, pp. 7–12.
10. L. Garcia Aranda, Y. Chastel, J. Fernández Pascual, and T. Dal Negro: *Adv. Technol. Plast.*, 2002, vol. 2 (2002), pp. 1135–40.
11. G. Berglund: *First International Conference on Hot Sheet Metal Forming of High Performance Steel*, Kassel, Germany (2008), pp, 175–77.
12. D.W. Fan, H.S. Kim, and B.C. De Cooman: *Steel Res. Int.*, 2009, vol. 80, pp. 241–48.
13. H. Karbasian and A.E. Tekkaya: *J. Mater. Process. Technol.*, 2010, vol. 210, pp. 2103–18.
14. D.W. Fan and B.C. De Cooman: *Steel Res. Int.*, 2012, vol. 83, pp. 412–33.
15. E. Almeida: *Ind. Eng. Chem. Res.*, 2001, vol. 40, pp. 3–14.
16. E. Almeida: *Ind. Eng. Chem. Res.*, 2001, vol. 40, pp. 15–20.
17. L. Dosdat, J. Petitjean, T. Vietoris, and O. Clauzeau: *Steel Res. Int.*, 2011, vol. 82, pp. 726–33.
18. D.W. Fan and B.C. De Cooman: *ISIJ Int.*, 2010, vol. 50, pp. 1713–18.
19. M. Windmann, A. Röttger, and W. Theisen: *Surf. Coat. Technol.*, 2014, vol. 246, pp. 17–25.
20. C. Allély, L. Dosdat, O. Clauzeau, K. Ogle, and P. Volovitch: *Surf. Coat. Technol.*, 2014, vol. 238, pp. 188–96.
21. K. Uda, A. Azushima, and A. Yanagida: *J. Mater. Process. Technol.*, 2016, vol. 228, pp. 112–16.
22. Z.X. Gui, W.K. Liang, Y. Liu, and Y.S. Zhang: *Mater. Des.*, 2014, vol. 60, pp. 26–33.
23. J. Mackowiak and N. Short: *Int. Met. Rev.*, 1979, vol. 24, pp. 1–19.
24. A. Marder: *Prog. Mater. Sci.*, 2000, vol. 45, pp. 191–271.
25. R. Autengruber, G. Luckeneder, S. Kolnberger, J. Faderl, and A.W. Hassel: *Steel Res. Int.*, 2012, vol. 83, pp. 1005–11.
26. R. Autengruber, G. Luckeneder, and A.W. Hassel: *Corros. Sci.*, 2012, vol. 63, pp. 12–19.
27. C.W. Lee, W.S. Choi, Y.R. Cho, and B.C. De Cooman: *ISIJ Int.*, 2014, vol. 54, pp. 2364–68.
28. O.L. Ighodaro, E. Biro, and Y.N. Zhou: *J. Mater. Process. Technol.*, 2016, vol. 236, pp. 64–72.
29. C.W. Ji, I. Jo, H. Lee, I.D. Choi, Y. do Kim, and Y.D. Park: *J. Mech. Sci. Technol.*, 2015, vol. 28, pp. 4761–69.
30. C.W. Lee, D.W. Fan, I.R. Sohn, S.J. Lee, and B.C. De Cooman: *Metall. Mater. Trans. A*, 2012, vol. 43A, pp. 5122–27.
31. C.W. Lee, W.S. Choi, L. Cho, Y.R. Cho, and B.C. De Cooman: *ISIJ Int.*, 2015, vol. 55, pp. 264–71.
32. L. Cho, H. Kang, C. Lee, and B.C. De Cooman: *Scripta Mater.*, 2014, vols. 90–91, pp. 25–28.

33. H. Kang, L. Cho, C. Lee, and B.C. De Cooman: *Metall. Mater. Trans. A*, 2016, vol. 47A, pp. 2885–2905.
34. J. Selverian, M. Notis, and A. Marder: *J. Mater. Eng.*, 1987, vol. 9, pp. 133–40.
35. Y.H. Leng, Y.L. Feng, and M. Song: *Adv. Mater. Res.*, 2012, vol. 415, pp. 276–80.
36. H. Fujsawa, R. Kaneko, and H. Ishikawa: *JFE Tech. Rep.*, 2009, vol. 14, pp. 41–45.
37. S.F. Radtke and D.C. Herrschaft: *J. Less-Common Met.*, 1982, vol. 93, pp. 253–59.
38. F. Rosalbino, E. Angelini, D. Maccio, A. Saccone, and S. Delfino: *Electrochim. Acta*, 2007, vol. 52, pp. 7107–14.
39. B. Zhou, F. Jin, Q. Luo, Q. Li, and K.C. Chou: *Adv. Mater. Res.*, 2011, vols. 399–401, pp. 1998–2003.
40. C.W. Lee and B.C. De Cooman: *Metall. Mater. Trans. A*, 2014, vol. 45A, pp. 4499–4509.
41. C.W. Lee, W.S. Choi, Y.R. Cho, and B.C. De Cooman: *Surf. Coat. Technol.*, 2015, vol. 281, pp. 35–43.
42. ASTM E21: *Standard Test Methods for Elevated Temperature Tension Tests of Metallic Materials*, ASTM International, Philadelphia, 2003.
43. ASTM E8/E8M: *Standard Test Methods for Tension Testing of Metallic Materials*, ASTM International, Philadelphia, 2003.
44. ICDD: *PDF-2 2002 Database*, International Centre for Diffraction Data, Newtown Square, PA, 2002.
45. J.K. Chang and C.S. Lin: *Metall. Mater. Trans. A*, 2017, vol. 48A, pp. 3734–44.
46. M. Żelechower, J. Kliś, E. Augustyn, J. Grzonka, D. Stróż, T. Rzychoń, and H. Woźnica: *Arch. Metall. Mater.*, 2012, vol. 57, pp. 517–23.
47. S. Shibli, B. Meena, and R. Remya: *Surf. Coat. Technol.*, 2015, vol. 262, pp. 210–15.
48. W.D. Callister and D.G. Rethwisch: *Materials Science and Engineering*, 9th ed., Wiley, Hoboken, 2015, pp. 19–55.
49. J. Kondratiuk, P. Kuhn, E. Labrenz, and C. Bischoff: *Surf. Coat. Technol.*, 2011, vol. 205, pp. 4141–53.
50. T. Mörtlbauer, S. Kolnberger, and J. Faderl: *Galvatech'15 Proceedings*, Toronto, Canada, 2015, pp. 861–67.
51. X. Hu and T. Watanabe: *Nano Plating-Microstructure Formation Theory of Plated Films and a Database of Plated Films*, 1st ed., Elsevier, Oxford, 2004, pp. 577–88.
52. R. Bensalem, O. Guergueb, S. Alleg, A. Younes, S. Souilah, M. Bououdina, and J. Suñol: *Proc. Int. Conf. Nanomater.: Appl. Prop.*, 2013, vol. 2, pp. 02PCN12-01–02PCN12-04.
53. V. Janik, Y. Lan, P. Beentjes, D. Norman, G. Hensen, and S. Sridhar: *Metall. Mater. Trans. A*, 2015, vol. 47A, pp. 400–11.
54. M. Tumuluru: *Weld. J.*, 2007, vol. 86, pp. 161–69.
55. H. Lee and D. Hiam: *Corrosion*, 1989, vol. 45, pp. 852–56.
56. X. Zhang and I. Bravo: *Corrosion*, 1994, vol. 50, pp. 308–17.
57. M. Nicholas and C. Old: *J. Mater. Sci.*, 1979, vol. 14, pp. 1–18.
58. P. Fernandes and D. Jones: *Int. Mater. Rev.*, 1997, vol. 42, pp. 251–61.
59. E. Tada and Y. Miura: *ISIJ Int.*, 2016, vol. 56, pp. 444–51.
60. T.H. Shen, C.Y. Tsai, and C.S. Lin: *Surf. Coat. Technol.*, 2016, vol. 306, pp. 455–61.
61. W. Chen, Q. Liu, Q. Liu, L. Zhu, and L. Wang: *J. Alloy Compd.*, 2008, vol. 459, pp. 261–66.
62. M.M. Sadawy: *Am. J. Mater. Res.*, 2014, vol. 4, pp. 53–58.
63. J. Masalski, J. Gluszek, J. Zabrzeski, K. Nitsch, and P. Gluszek: *Thin Solid Films*, 1999, vol. 349, pp. 186–90.
64. M. Budinski and B. Wilde: *Corrosion*, 1987, vol. 43, pp. 60–62.
65. A.S. Khanna: *Introduction to High Temperature Oxidation and Corrosion*, ASM International, Materials Park, 2002, pp. 80–81, 109–34.
66. D.R. Gaskel: *Introduction to the Thermodynamics of Materials*, CRC Press, Boca Raton, FL, 2008, pp. 305–586.
67. B. C. De Cooman, W. Jung, K. R. Jo, D. H. Sulistiyo, L. Cho: *Galvatech 2017 Conf.*, Tokyo, Japan, 2017, pp. 790–95.
68. K.L. Lin, C.F. Yang, and J.T. Lee: *Corrosion*, 1991, vol. 47, pp. 9–17.
69. K.L. Lin, C.F. Yang, and J.T. Lee: *Corrosion*, 1991, vol. 47, pp. 17–23.
70. C.J. Boxley, J.J. Watkins, and H.S. White: *Solid-State Lett.*, 2003, vol. 6, pp. B38–B41.
71. A.M. Lazar, W.P. Yespica, S. Marcelin, N. Pébère, D. Samélor, C. Tendero, and C. Vahlas: *Corros. Sci.*, 2014, vol. 81, pp. 125–31.